A&A 416, 655–659 (2004)
DOI: 10.1051/0004-6361:20034419
© ESO 2004

Astronomy & Astrophysics

# Atomic lines in infrared spectra for ultracool dwarfs*,**

Y. Lyubchik[1], H. R. A. Jones[2], Y. V. Pavlenko[1], S. Viti[3,4], J. C. Pickering[5], and R. Blackwell-Whitehead[5]

[1] Main Astronomical Observatory of Academy of Sciences of Ukraine, Golosiiv woods, Kyiv-127, 03680 Ukraine
[2] Astrophysics Research Institute, Liverpool John Moores University, Twelve Quays House, Egerton Wharf, Birkenhead CH41 1LD, UK
[3] CNR-Instituto di Fisica dello Spazio Interplanetario, Area di Ricerca di Tor Vergata, via del fosso del Cavaliere 100, 00133 Roma, Italy
[4] Dept of Physics and Astronomy, University College London, Gower St., London WC1E 6BT, UK
[5] Blackett Laboratory, Imperial College, Prince Consort Rd, London SW7 2BW, UK

Received 30 September 2003 / Accepted 26 November 2003

**Abstract.** We provide a set of atomic lines which are suitable for the description of ultracool dwarf spectra from 10 000 to 25 000 Å. This atomic linelist was made using both synthetic spectra calculations and existing atlases of infrared spectra of Arcturus and Sunspot umbra. We present plots which show the comparison of synthetic spectra and observed Arcturus and Sunspot umbral spectra for all atomic lines likely to be observable in high resolution infrared spectra.

**Key words.** infrared: stars – stars: low mass – brown dwarfs – atomic data

## 1. Introduction

Ultracool dwarfs extend from the cool M dwarfs into the brown dwarf regime and include the spectral types L and T. It is likely that most of the ultracool dwarfs are not massive enough to undergo nuclear fusion in their cores to burn hydrogen and are thus brown dwarfs rather than stars. Here we are concerned in general terms with the spectroscopy of cool objects and use the broad temperature classification "ultracool dwarf" in preference to more specific terms with a physical meaning such as M dwarf and brown dwarf (Jones & Steele 2001).

The astrophysical importance of ultracool dwarf stars derives from the large-scale cosmological significance of their mass density, to their extremely slow chemical evolution and to their formation process and their distinction from planets. Ultracool dwarfs span the mass range from the coolest stars through two orders of magnitude in mass to giant planets. By determining their fundamental parameters, such as effective temperature, metallicity and surface gravity, their position in the Hertzsprung-Russell diagram can be determined. So far these parameters, in particular surface gravity and metallicity, are poorly determined. Yet to derive a reliable mass function across the brown dwarf regime and to discern the abundance patterns of low-metallicity brown dwarfs, it is essential to design much finer tools of analysis. Changes in effective temperatures, surface gravity and metallicity can lead to similar spectral changes. To disentangle these effects requires observations of several spectral diagnostics that respond differently to changes in these parameters (e.g., Reid & Hawley 2000).

Colour information has proved crucial in the identification of most ultracool dwarfs. However, their complex energy distributions mean that colours do not change monotonically with changing luminosity and temperature. This makes differentiation of second order effects such as metallicity and gravity very difficult to discern. Spectroscopic observations are crucial and low-mass objects have been successfully classified both in the optical (Kirkpatrick et al. 2000; Basri et al. 2000) and infrared (McLean et al. 2001; Geballe et al. 2001; Leggett et al. 2001) regimes across the M and L spectral classes. However by the T spectral class there is insufficient flux at short wavelengths to use optical wavelengths. Furthermore even by the early L spectral class the energy distribution at optical wavelengths is almost completely dominated by broad alkali resonance lines and dust opacities (Pavlenko 1998; Pavlenko et al. 2000; Burrows et al. 2000; Tsuji 2002). The infrared region is also difficult to model with strong molecular opacities of water, iron hydride and at cooler temperatures methane as well. However, there are also a number of atomic lines observable in the infrared spectra of ultracool dwarfs (e.g. McLean et al. 2003). These infrared atomic lines lie across the peak in energy

---

*Send offprint requests to*: Y. Lyubchik,
e-mail: `lyu@mao.kiev.ua`

* Figure 1 is only available in electronic form at `http://www.edpsciences.org`

** Tables 1 and 2 are only available in electronic form at the CDS via anonymous ftp to `cdsarc.u-strasbg.fr (130.79.128.5)` or via `http://cdsweb.u-strasbg.fr/cgi-bin/qcat?J/A+A/416/655` distribution for these stars and are thus comparatively easier to observe than lines of the same atoms in the visible.

In recent years there has been a focus on improvements to the atomic data in the optical region, e.g., NIST (Kelleher et al. 1999), Opacity Project (Seaton et al. 1992). However, currently the accuracy and completeness of the atomic data, in particular oscillator strengths, in the IR region are far poorer. In many cases either the oscillator strengths are highly inaccurate or there are simply no measurements available. This becomes evident when synthetic spectra are generated to match infrared spectra, e.g., Jones et al. (1996), Jones & Viti (2000). Here we identify suitable sensitive infrared atomic lines that may one day be used for reliable temperature, gravity and abundance analyses for a wide range of ultracool dwarfs, from M dwarf stars through brown dwarfs as well as extra-solar giant planets. Our paper is the first step in the development of a database of infrared atomic lines with reliable oscillator strengths suitable for the study of low temperature astrophysical objects. Our specific focus is the interpretation of ultracool dwarfs covering the temperature space from the M dwarfs through the brown dwarfs to extra-solar giant planets.

Our focus is the prioritisation of atomic lines whose oscillator strengths we are either already measuring or planning to measure. Section 2 describes the observational material, atomic line lists and theoretical spectra necessary for this study. Our procedures for identifying important infrared atomic transitions are discussed in Sect. 3. In Sect. 4 we discuss our results and conclusions. In Sect. 5 we outline our plans for experimental measurements of the atomic data.

## 2. Input datasets

### 2.1. Observed spectra of Arcturus and Sunspot umbra

For comparisons and the robust identification of atomic lines we used both electronic and hard copies of the "Infrared Atlas of the Arcturus spectrum, 0.9–5.3 $\mu$m" (hereafter "Arcturus atlas") (Hinkle et al. 1995) and "An Atlas of a Dark Sunspot Umbral spectrum from 1970 to 8640 cm$^{-1}$ (1.16 to 5.1 $\mu$m)" (hereafter "Sunspot umbra atlas") (Wallace & Livingston 1992). We used the electronic versions of both atlases (`ftp://ftp.noao.edu/catalogs/arcturusatlas/ir/` and `ftp://ftp.noao.edu/fts/spot1atl/`) to compare with our synthetic spectra.

Arcturus ($\alpha$ Boo) is a K1 III star of effective temperature $T_{\rm eff} = 4300 \pm 30$ K and log $g = 1.5 \pm 0.15$ (Peterson et al. 1993). These parameters are far from adequate to describe ultracool dwarf atmospheres ($T_{\rm eff} \leq 2600$ K, log $g \sim 4.5$–$5.0$) though the Arcturus atlas provides careful identification of atomic lines and gives an opportunity to assess the behaviour of atomic lines when decreasing effective temperature from 4000 K to 2000 K. The atlas contains winter and summer observations. Since only the telluric spectrum is affected by seasons, in this paper we only use the telluric free summer data. The resolution of this atlas is of the order of $R \sim 100\,000$. The presence of a magnetic field in Arcturus is indirectly confirmed by strong emission lines in the ultraviolet spectral region formed in chromosphere of Arcturus (Ayres et al. 1986). However the average value of the magnetic field is, probably, similar to the solar one, since atomic line splitting is not seen in the observed sprectrum.

The Sunspot umbra atlas has a spectral type of M2–M5 V, which corresponds to an effective temperature range of around $T_{\rm eff} = 3170$–$3520$ K (Wallace & Livingston 1992; Viti et al. 1998). The magnetic field strength is estimated as $\approx$3360 Gauss. Due to the position of the umbra near the centre of the solar disk we see only $\sigma$-components of Zeeman split lines of large Lande factor $g$ in the Sunspot umbra atlas. Due to the strong magnetic field in the spot most of the atomic lines in the Sunspot umbral spectrum have doublet-like profiles. Molecular lines, with few exceptions, are magnetically insensitive and show single profiles. The Sunspot umbra atlas provides a spectrum corrected for atmospheric absorption. Its resolution is $R \sim 200\,000$ between 10 000 and 25 000 Å.

### 2.2. Synthetic spectra

Computations of synthetic spectra were carried out using the WITA6 program (Pavlenko 2000) assuming Local Thermodynamic Equilibrium.

For the computation of synthetic specta we used the NextGen model atmospheres structures (Hauschildt, private communication; Hauschildt et al. 1999) for cool spectra, and model atmosphere structures of Kurucz (1994) for the higher temperature synthetic spectra of Arcturus.

The atomic linelist used for our spectral modeling and line identification was taken from the VALD database (Kupka et al. 1999). VALD is a compilation of several different lists of atomic line data which were obtained from experimental measurements and theoretical calculations by various authors.

Chemical equilibria were computed for the mix of around 100 molecular species. Input molecular data and continuum opacity sources are described elsewhere (Pavlenko et al. 1995; Pavlenko 1997, 2000). The profiles of absorption lines are described by the Voigt function $H(a, v)$. The formulae of Unsold (1955) were used for calculation of damping constants. For these model atmospheres we adopt the conventional value of microturbulent velocity $v_{\rm t} = 2$ km s$^{-1}$. Theoretical spectra were computed with a wavelength step of 0.05 Å and then convolved with Gaussians to match the instrumental broadening.

We should note, that we didn't consider dusty effects in our synthetic spectra calculations, since the main purpose of the present work was not to model the real spectra of ultracool objects, but to reveal the prominent atomic features to be observed in such objects. The effects of dust will modify atomic line strengths in ultracool dwarf spectra. But dust will not affect the quantum-mechanical parameters which we intend to measure at the present time.

## 3. Procedure

Our procedure of line identification and selection is based on the comparison of synthetic spectra with the observed spectra of Arcturus and Sunspot umbra from 10 000 to 25 000 Å.

For ultracool dwarfs we used only synthetic spectra. The choice of model atmosphere parameters was aimed at obtaining a reliable atomic line list for ultracool dwarfs in the IR region. A model atmosphere of $T_{\rm eff}/\log g/[{\rm M/H}] = 2000/5.0/0.0$ was selected (hereafter "ultracool dwarf model"). This corresponds to an ultracool dwarf spectral class of around L0 (Kirkpatrick et al. 1999; Martin et al. 1999). The half width of the Gaussian we used to account for instrumental broadening in the "ultracool dwarf" synthetic spectrum is 0.4 Å which corresponds to resolution $R \sim 20\,000$–$40\,000$, approximately the resolution available to modern infrared echelle spectrometers operating between 10 000–25 000 Å. Another model atmosphere 4000/4.5/0.0 (hereafter "Arcturus-like model") was chosen to select some observable spectral atomic features formed in hotter atmospheres. The half width of the Gaussian for this synthetic spectrum is 0.13 Å to match the line broadening by macroturbulent velocity $\upsilon_{\rm macro} = 3.5$ km s$^{-1}$ in the Arcturus spectrum (Peterson et al. 1993). The $T_{\rm eff} = 4000$ K is slightly lower than Arcturus $T_{\rm eff} = 4300$ K (Peterson et al. 1993), and higher than the temperature of the Sunspot umbra $T_{\rm eff} \sim 3170$–$3520$ K (Wallace & Livingston 1992).

In the electronic versions of the Arcturus and Sunspot umbra atlases the data are given on a wavenumber scale. We transform the wavenumbers to wavelengths in air using the formula from Allen's Astrophysical Quantities (2000).

It is well known that the difficulties of line identification in IR spectra of ultracool dwarfs have a number of causes. There are many strong molecular lines of $H_2O$ (Jones et al. 2002), FeH (Cushing et al. 2003), CO (Pavlenko & Jones 2003), $CH_4$ (Noll et al. 2000) native to ultracool dwarfs as well as telluric molecular lines, particularly strong between the $J$, $H$ and $K$ bands. Nevertheless, we were able to identify many absorption features in the atmospheres of Arcturus and Sunspot umbra spectra likely to be present in ultracool dwarfs. To do this, we developed a procedure based on the inter-comparison of computed and observed spectra designed to minimise possible errors in line identification. The line identification files were made using:

a) "ultracool dwarf" synthetic spectrum (2000/5.0/0.0);
b) "Arcturus-like" synthetic spectrum (4000/4.5/0.0).

In addition we used line identification files from hard copy Arcturus and Sunspot umbra atlases.

In our identification procedure we assume that lines absorb only at a given wavelength. This assumption provides an upper limit of absorption. In the real spectra the residual intensity may be lower due to contribution of other lines. For every line from the VALD linelist in the range of 10 000–25 000 Å the residual flux $r_\nu = \frac{(\text{Flux in line})_\nu}{(\text{Flux in continuum})_\nu}$ was computed. Atomic lines from VALD with central intensities deeper than 0.8 of the residual flux in the spectrum of 2000/5.0/0.0 atmosphere were selected to restrict the number of lines to those likely to be observable in cool spectra. These lines are given in the Table 1. The set of the selected lines is rather large and thus we assign different levels of priority to the lines. The main criteria for selecting lines of the highest priority is that the central intensity of the identified line ought to be greater than 0.6 of the residual flux (Col. 4 in the Table 1) in the "ultracool dwarf" synthetic spectrum.

Plots for all spectral regions containing atomic lines of interest are shown in Fig. 1 (they are also available at `http://www.astro.livjm.ac.uk/~hraj/spectralatlas/index.html`). The identifications of atomic features are labelled in the spectra. Arrows and labels at the top of the plots show identification in the "ultracool dwarf" synthetic spectrum, the same labels in the bottom of the plots are for the "Arcturus-like" spectrum. The Sunspot umbral spectrum is shown by bold line, the Arcturus spectrum by a dotted line, the "ultracool dwarf" synthetic spectrum as a solid line and "Arcturus-like" synthetic spectrum as a dashed line. In order to simplify our plots molecular line identifications are not included. Usually molecular lines have narrow deep profiles allowing them to be distinguished from atomic lines. Their identification in the Sunspot umbra and Arcturus can be found in the hard copy atlases.

## 4. Results

Our results are shown in two tables. Table 1 contains all identified lines with central intensities deeper than 0.8 of residual flux using "ultracool dwarf model" identifications. Table 2 investigates the sensitivity of priority 1 lines identified in Table 1 to temperature, gravity and metallicity.

In the first column of Table 1 we estimate the priority of lines for measurement of atomic data.

a) Priority 1 indicates that the atomic line is deeper than 0.6 in the 2000/5.0/0.0 synthetic spectrum. Also we include as first priority three lines of Ti (22211.229, 22232.838, 22274.012 Å) which are shallower than 0.6. They are located far from strong atomic and molecular lines and thus are good for identification purposes in the spectra of ultracool dwarfs.
b) Priority 2 indicates that the residual flux of an atomic line is between 0.8–0.6.
c) Priority 3 indicates that the atomic line is located in the wing of a nearby stronger line or in a wavelength region with strong telluric absorption.

Atomic lines without an assigned priority might be relevant in the analysis of ultracool dwarf spectra, but they are predicted to be weak in the synthetic spectrum.

The second column shows the wavelength of the line in Å in air. These values were taken from VALD. We check that wavelengths from Arcturus and Sunspot umbra atlases identification files are in a good agreement with VALD. The wavelengths of a few lines differ from VALD values by less than 0.1 Å in the region 10 000–20 000 Å and by less than 0.3 Å beyond 20 000 Å.

The third column shows the atomic identifications of the line.

Columns 4–7 show the linedepths of identified lines. Column 4 – the residual flux in the line obtained from the "ultracool dwarf" synthetic spectrum; Col. 5 – from the "Arcturus-like" synthetic spectrum; Col. 6 – measured from the hard copy of Arcturus atlas depth of identified atomic lines; Col. 7 – the same as Col. 6 for the hard copy of the Sunspot umbra atlas. As was mentioned above we used the hard copy versions of the Arcturus and Sunspot umbra atlases to measure linedepths.

The accuracy of our line depth measurements from the hardcopy atlases is ~0.01–0.02 for the Arcturus atlas (Col. 6) and ~0.02–0.03 for the Sunspot umbra atlas (Col. 7). We note that linedepth information given in Cols. 6 and 7 is only used to check the presence of a line in the observed spectra. Thus we do not need high accuracy linedepth measurements for the observable spectra of the Sunspot umbra and Arcturus.

We note that the data in the Sunspot umbra atlas provide a spectrum from 11 600 Å, rather than 10 000 Å where our figures and tables start from. Some lines are labelled (see Col. 7) by the symbol "~" which means that part of the line in the hard copy of the atlas is obscured by a gap in the data and the value given in the table is for the visible part of the line. In Cols. 6 and 7 there are also some lines with "bl" suffices. This means that these lines are blended with stronger nearby lines.

There are two regions with strong telluric absorption (marked in Cols. 6 and 7 by $\bigoplus$): 13 600–14 770 Å and 18 260–19 450 Å, regions between the $J$ and $H$, and $H$ and $K$ photometric bands. Lines identified from VALD in these regions are difficult to observe in ground based observations but can be used in probable future space observations of ultracool dwarfs.

Finally we note, that in Table 1 we italicise atomic lines of Rb, Y, Ba and Lu, identified only using theoretical computations. Although these lines are not seen in the observations of Arcturus and Sunspot umbra, they are strong in the synthetic spectrum computed for the 2000/5.0/0.0 model atmosphere, and therefore also likely to be strong below 2000 K.

In Table 2 we show only lines which were marked in Table 1 as first priority lines. The first column are wavelengths in Å; the second column are names of elements. In the third column we give the central line intensity for the "ultracool dwarf" (2000/5.0/0.0) spectrum. We compute some synthetic spectra for ultracool objects varying parameters of $T_{\rm eff}$, log $g$ and metallicity to show the sensitivity of the central intensities of identified lines to these parameters. For our computations we chose the minimal step in model atmospheres grid: $\Delta T_{\rm eff} = 100$ K, $\Delta \log g = 0.5$, $\Delta$[M/H] = −0.5. In Cols. 4–6 we show the difference of central intensity (in %) computations with "new" models from central intensity computations for our "ultracool dwarf model". Negative values in Cols. 4–6 indicate that a line is stronger in the new model relative to the reference model 2000/5.0/0.0.

Column 4 shows the dependence of residual fluxes on effective temperature. For comparison a 2100/5.0/0.0 synthetic spectrum was used. One can see that only a few lines show strong temperature dependence for $\Delta T_{\rm eff} = 100$ K. The NextGen 2000/4.5/0.0 model was used with 2000/5.0/0.0 to test gravity sensitivity. The dependence for $\Delta(\log g) = 0.5$ is also relatively weak for most lines and is shown in Col. 5. $\Delta$[M/H] = 0.5 from computations using NextGen model atmospheres 2000/5.0/-0.5 and 2000/5.0/0.0 is shown in Col. 6. The metallicity dependence is relatively high for all lines. Thus Table 2 indicates that relatively small variations of model atmosphere parameters will not seriously affect our line selection and prioritisation.

## 5. Experimental work

The identification and prioritisation of atomic lines presented in this paper is only the first step in our project and is primarily based on a theoretical treatment. Our program of measurements of atomic data for the priority lines given in this paper is underway. We are currently measuring oscillator strengths by measurements of sets of relative line intensities using the high resolution Fourier transform spectrometers at Imperial College (Pickering 2002) and NIST (National Institute of Standards and Technology, US). We have already recorded spectra of Ti, Mn and Na, and measurements of Mg, K, Ca and Fe are in progress. Measurements of other species listed in Table 1 are underway in the near future. These line intensities will be used to obtain branching ratios which are then combined with level lifetimes to obtain $f$-values. We expect to achieve uncertainties in $f$-values of around 10–15%.

*Acknowledgements.* We would like to thank the authors of the Arcturus and Sunspot umbra atlases for making their data available through an ftp site and Prof. Hauschildt and the PHOENIX team for NextGen model atmospheres. NSO/Kitt Peak FTS data used here were produced by NSF/NOAO. S.V. thanks the Italian Space Agency (ISA) for financial support. RBW thanks Gillian Nave at NIST for the assistance and facilities provided for the IR experimental measurements. All the authors thank the Royal Society and PPARC of the UK for support of travel and experimental work.

## References

Allen's Astrophysical Quantities 2000 (Springer)

Ayres, T. R., Judge, P., Jordan, C., Brown, A., & Linsky, J. L. 1986, ApJ, 311, 947

Basri, G., Mohanty, S., Allard, F., et al. 2000. ApJ, 538, 363

Burrows, A., Marley, M. S., & Sharp, C. M. 2000, ApJ, 531, 438

Cushing, M. C., Rayner, J. T., Davis, S. P., & Vacca, W. D. 2003, ApJ, 582, 1066

Geballe, T. R., Saumon, D., Leggett, S. K., et al. 2001, ApJ, 556, 373

Hauschildt, P. H., Allard, F., & Baron, E. 1999, ApJ, 512, 377

Hinkle, K., Wallace, L., & Livingston, W. 1995, Infrared Atlas of the Arcturus Spectrum, 0.9–5.3 microns, Book Crafters Inc., 372

Jones, H. R. A., Longmore, A. J., Allard, F., & Hauschildt, P. H. 1996, MNRAS, 280, 77

Jones, H. R. A., & Viti, S. 2000, ISO beyond the peaks: The 2nd ISO workshop on analytical spectroscopy, ESA-SP 456

Jones, H. R. A., & Steele, I. A. 2001, Ultracool Dwarfs: New spectral Types L and T, ed. H. R. A. Jones, & I. A. Steele (Berlin, Heidelberg: Springer)

Jones, H. R. A., Pavlenko, Ya., Viti, S., & Tennyson, J. 2002, MNRAS, 330, 675

Kelleher, D. E., Mohr, P. J., Martin, W. C., et al. 1999, SPIE, 3818, 170

Kirkpatrick, J. D., Reid, I. N., Liebert, J., et al. 1999. ApJ, 519, 802

Kirkpatrick, J. D., Reid, I. N., Liebert, J., et al. 2000. AJ, 120, 447

Kupka, F., Piskunov, N. E., Ryabchikova, T. A., Stempels, H. C., & Weiss, W. W. 1999, A&AS, 138, 119

Kurucz, R. L. 1994, CD-ROM No. 19

Leggett, S. K., Allard, F., Geballe, T. R., Hauschildt, P. H., & Schweitzer, A. 2001, ApJ, 548, 908

Martin, E., Delfosse, X., Basri, G., et al. 1999, AJ, 118, 2466

McLean, I. S., Prato, L., Kim, S. S., Burgasser, A. J., & Kirkpatrick, J. D. 2001, AAS, 198, No. 49.04

McLean, I. S., McGovern, M. R., Burgasser, A. J., et al. 2003, [`astro-ph/0309257`]

Noll, K. S., Geballe, T. R., Leggett, S. K., & Marley, M. S. 2000, ApJ, 541, 75

Pavlenko, Ya. V., Rebolo, R., Martin, E. L., & Garcia Lopez, R. J. 1995, A&A, 303, 807

Pavlenko, Ya. V. 1997, Ap&SS, 253, 43

Pavlenko, Ya. V. 1998, Astron. Rep., 42, 787

Pavlenko, Ya. V. 2000, Astron. Rep., 44, 219

Pavlenko, Y., Zapatero Osorio, M. R., & Rebolo, R. 2000, A&A, 355, 245

Pavlenko, Ya., & Jones, H. R. A. 2002, A&A, 396, 967

Peterson, R. C., Dalle Ore, C. M., & Kurucz, R. L. 1993, ApJ, 404, 333

Pickering, J. C. 2002, Vibrational Spectrosc., 29, 27

Reid, N., & Hawley, S. L. 2000, New light on dark stars: red dwarfs, low mass stars, brown dwarfs, ed. N. Reid, & S. L. Hawley (New York: Springer)

Tsuji, T. 2002, ApJ, 575, 264

Unsold, A. 1955, Physik der Sternatmospheren, 2nd ed. (Berlin: Springer)

Viti, S., Polyansky, O. L., Zobov, N. F., et al. 1998, ASP Conf. Ser., 154, CSSS, 718

Wallace, L., & Livingston, W. 1992, An Atlas of a Dark Sunspot Umbral Spectrum from 1970 to 8640 $\mathrm{cm}^{-1}$ (1.16 to 5.1 $\mu$m), NSO Technical Rep. No. 92-001

# Online Material

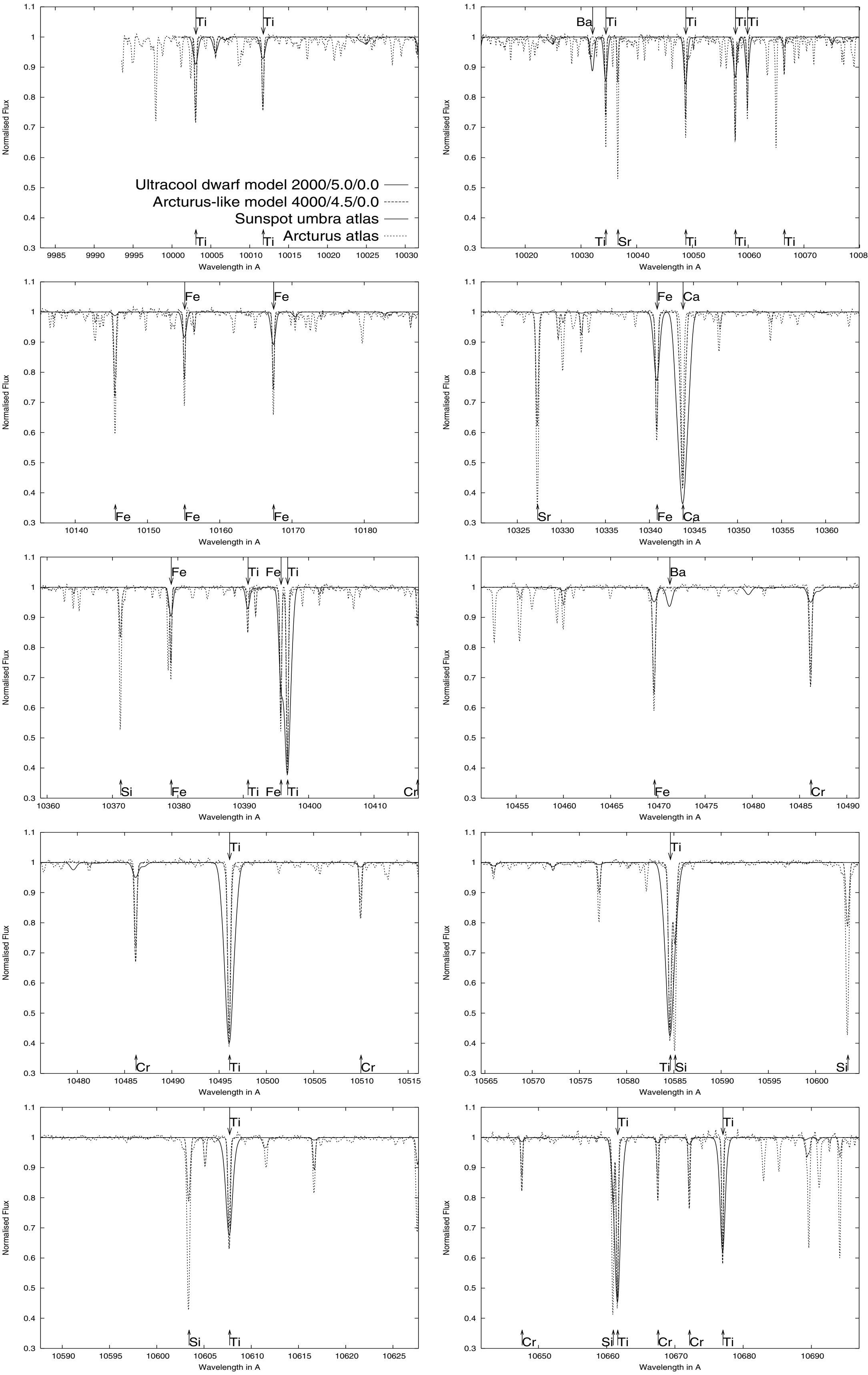

**Fig. 1.** Plots for all spectral regions containing atomic lines of interest in the 10 000–25 000 Å region. The identifications of atomic features are made by atomic name and arrows by the line of interest. Identification at the top of the plots is for the “ultracool dwarf” spectrum; identification at the bottom of the plots is for the “Arcturus-like” spectrum.

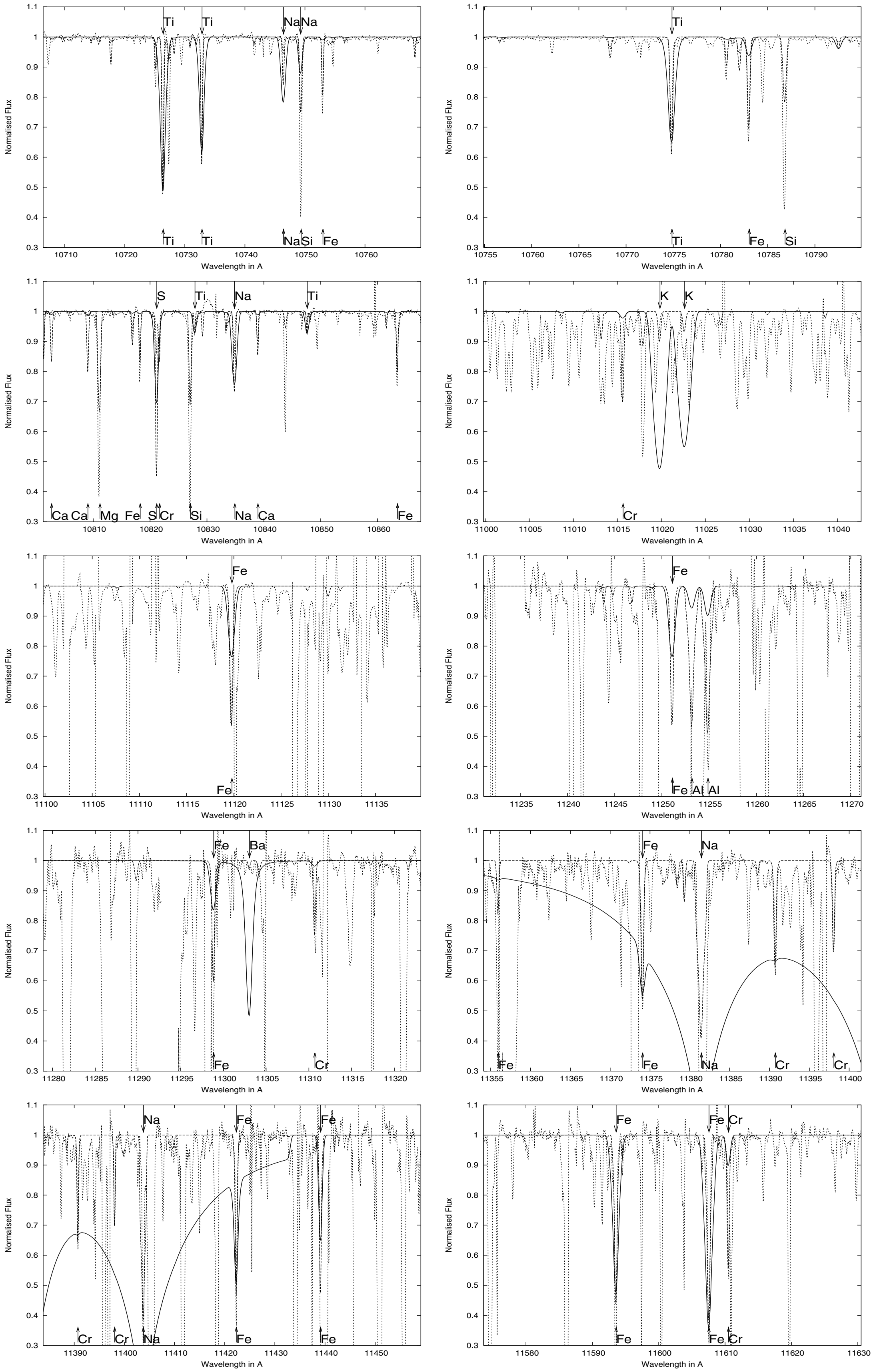
Normalised Flux
Wavelength in A
0.3
0.4
0.5
0.6
0.7
0.8
0.9
1
1.1
Ti
Ti
Na
Na
Ti
Ti
Na
Si
Fe
10710
10720
10730
10740
10750
10760
Ti
Ti
Fe
Si
10755
10760
10765
10770
10775
10780
10785
10790
S
Ti
Na
Ti
Ca
Ca
Mg
Fe
S
Cr
Si
Na
Ca
Fe
10810
10820
10830
10840
10850
10860
K
K
Cr
11000
11005
11010
11015
11020
11025
11030
11035
11040
Fe
Fe
11100
11105
11110
11115
11120
11125
11130
11135
Fe
Fe
Al
Al
11235
11240
11245
11250
11255
11260
11265
11270
Fe
Ba
Fe
Cr
11280
11285
11290
11295
11300
11305
11310
11315
11320
Fe
Na
Fe
Fe
Na
Cr
Cr
11355
11360
11365
11370
11375
11380
11385
11390
11395
11400
Na
Fe
Fe
Cr
Cr
Na
Fe
Fe
11390
11400
11410
11420
11430
11440
11450
Fe
Fe
Cr
Fe
Fe
Cr
11580
11590
11600
11610
11620
11630

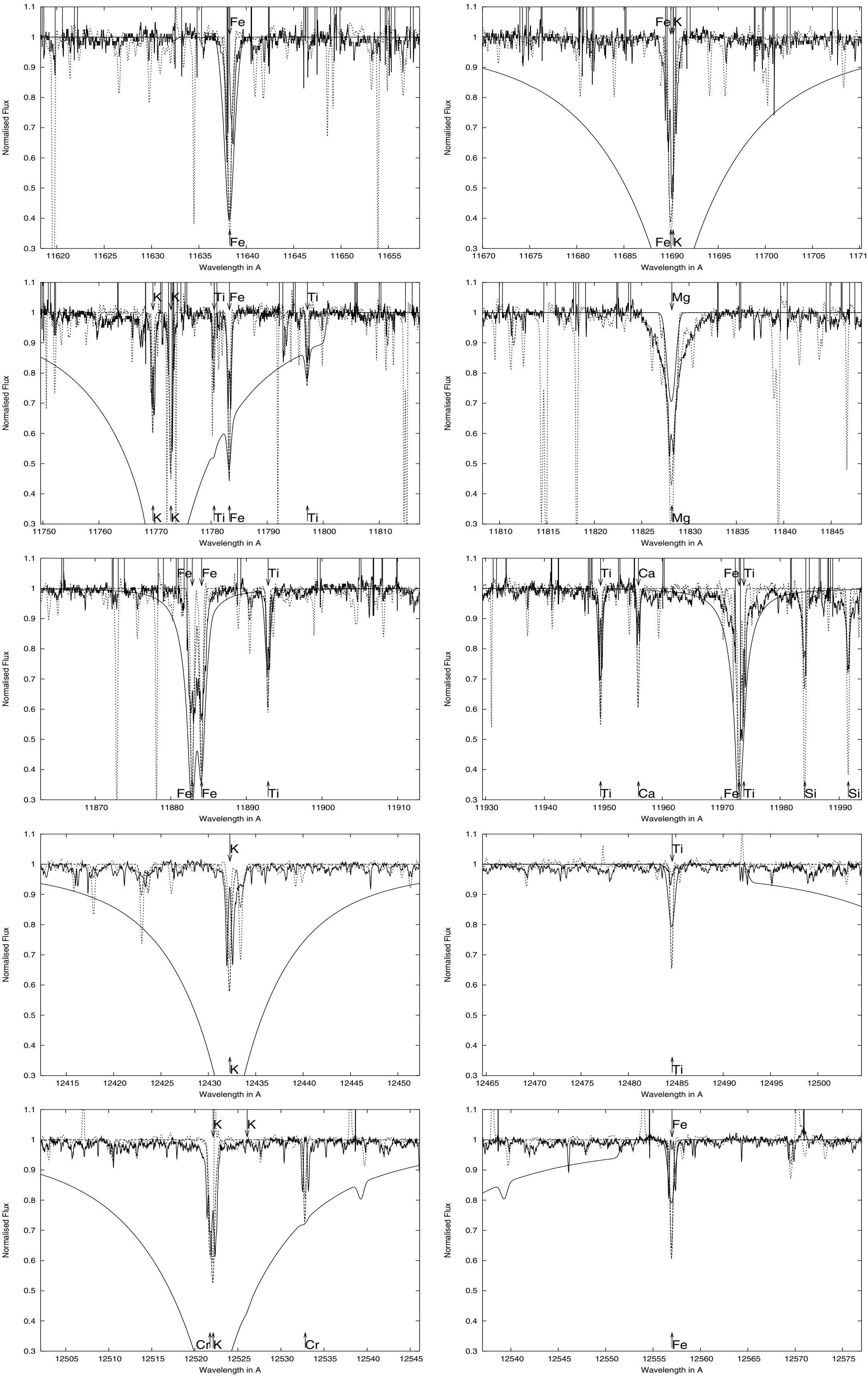
Normalised Flux
Wavelength in A
0.3
0.4
0.5
0.6
0.7
0.8
0.9
1
1.1
Fe
Fe
11620
11625
11630
11635
11640
11645
11650
11655
Fe K
Fe K
11670
11675
11680
11685
11690
11695
11700
11705
11710
K
K
Ti
Fe
Ti
K
K
Ti
Fe
Ti
11750
11760
11770
11780
11790
11800
11810
Mg
Mg
11810
11815
11820
11825
11830
11835
11840
11845
Fe
Fe
Ti
Fe
Fe
Ti
11870
11880
11890
11900
11910
Ti
Ca
Fe
Ti
Ti
Ca
Fe
Ti
Si
Si
11930
11940
11950
11960
11970
11980
11990
K
K
12415
12420
12425
12430
12435
12440
12445
12450
Ti
Ti
12465
12470
12475
12480
12485
12490
12495
12500
K
K
Cr
K
Cr
12505
12510
12515
12520
12525
12530
12535
12540
12545
Fe
Fe
12540
12545
12550
12555
12560
12565
12570
12575

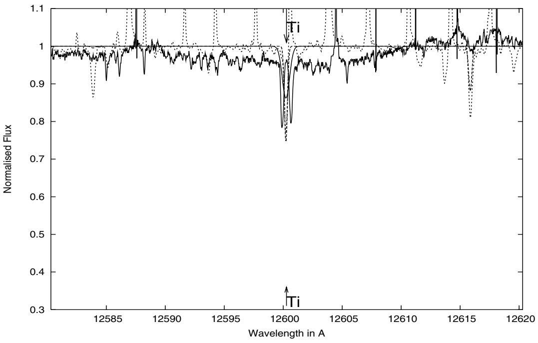
Ti
Ti
Normalised Flux
1.1
1
0.9
0.8
0.7
0.6
0.5
0.4
0.3
12585
12590
12595
12600
12605
12610
12615
12620
Wavelength in A

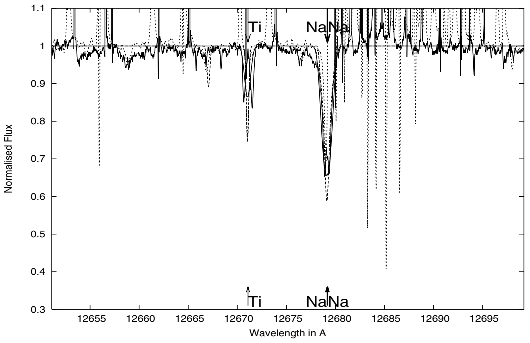
Ti
NaNa
Ti
NaNa
Normalised Flux
1.1
1
0.9
0.8
0.7
0.6
0.5
0.4
0.3
12655
12660
12665
12670
12675
12680
12685
12690
12695
Wavelength in A

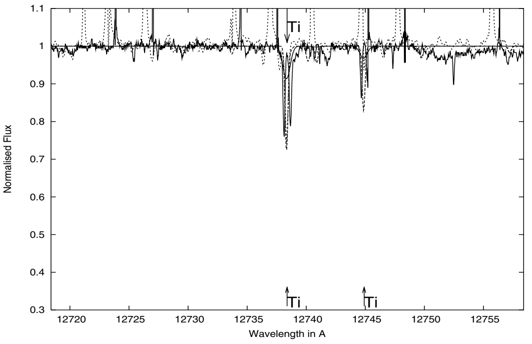
Ti
Ti
Ti
Normalised Flux
1.1
1
0.9
0.8
0.7
0.6
0.5
0.4
0.3
12720
12725
12730
12735
12740
12745
12750
12755
Wavelength in A

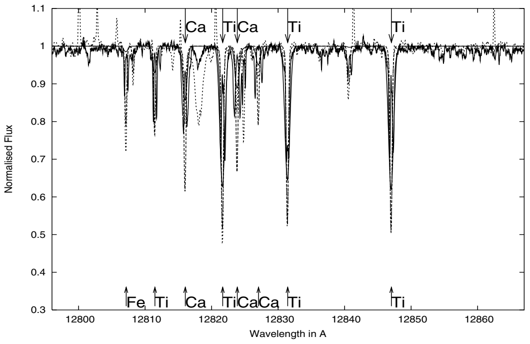
Ca
TiCa
Ti
Ti
Fe
Ti
Ca
TiCaCa
Ti
Ti
Normalised Flux
1.1
1
0.9
0.8
0.7
0.6
0.5
0.4
0.3
12800
12810
12820
12830
12840
12850
12860
Wavelength in A

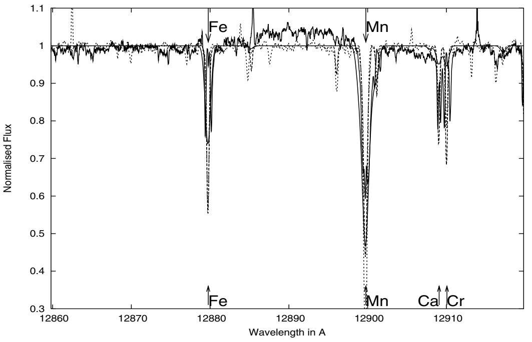
Fe
Mn
Fe
Mn
Ca
Cr
Normalised Flux
1.1
1
0.9
0.8
0.7
0.6
0.5
0.4
0.3
12860
12870
12880
12890
12900
12910
Wavelength in A

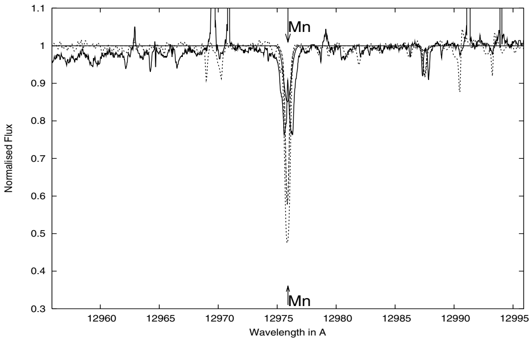
Mn
Mn
Normalised Flux
1.1
1
0.9
0.8
0.7
0.6
0.5
0.4
0.3
12960
12965
12970
12975
12980
12985
12990
12995
Wavelength in A

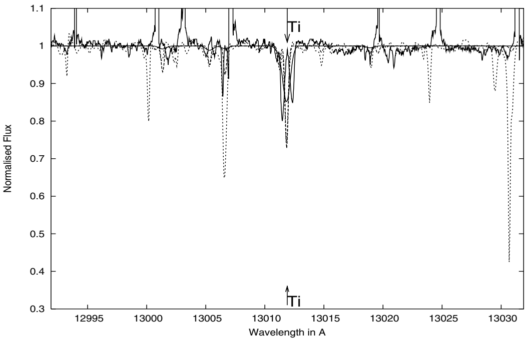
Ti
Ti
Normalised Flux
1.1
1
0.9
0.8
0.7
0.6
0.5
0.4
0.3
12995
13000
13005
13010
13015
13020
13025
13030
Wavelength in A

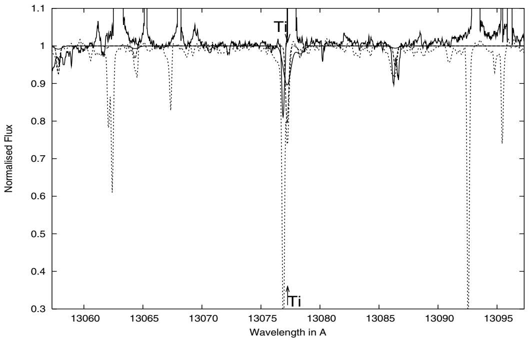
Ti
Ti
Normalised Flux
1.1
1
0.9
0.8
0.7
0.6
0.5
0.4
0.3
13060
13065
13070
13075
13080
13085
13090
13095
Wavelength in A

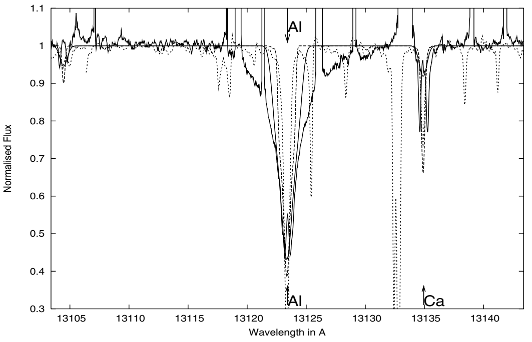
Al
Al
Ca
Normalised Flux
1.1
1
0.9
0.8
0.7
0.6
0.5
0.4
0.3
13105
13110
13115
13120
13125
13130
13135
13140
Wavelength in A

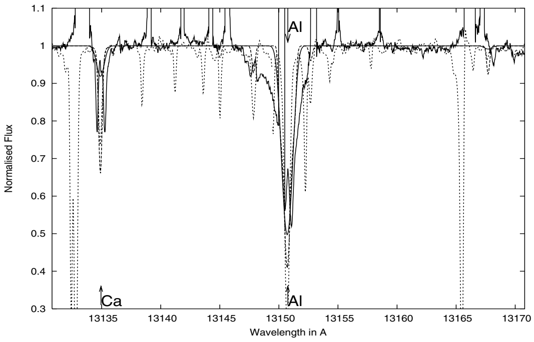
Al
Ca
Al
Normalised Flux
1.1
1
0.9
0.8
0.7
0.6
0.5
0.4
0.3
13135
13140
13145
13150
13155
13160
13165
13170
Wavelength in A

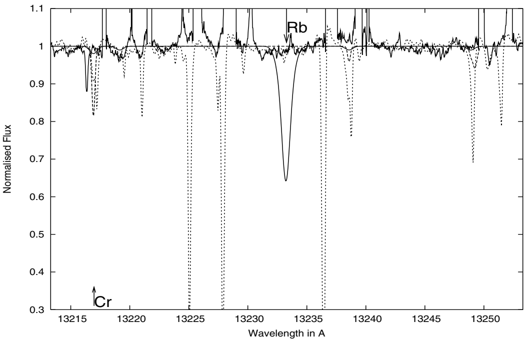
Rb
Cr
Normalised Flux
1.1
1
0.9
0.8
0.7
0.6
0.5
0.4
0.3
13215
13220
13225
13230
13235
13240
13245
13250
Wavelength in A

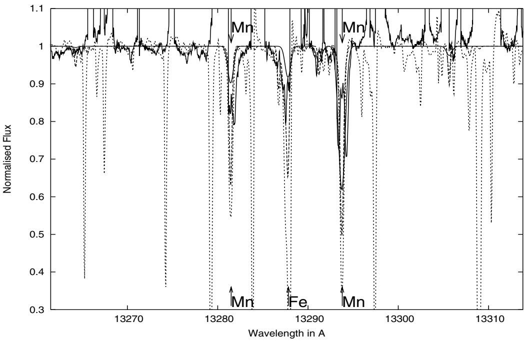
Mn
Mn
Mn
Fe
Mn
Normalised Flux
1.1
1
0.9
0.8
0.7
0.6
0.5
0.4
0.3
13270
13280
13290
13300
13310
Wavelength in A

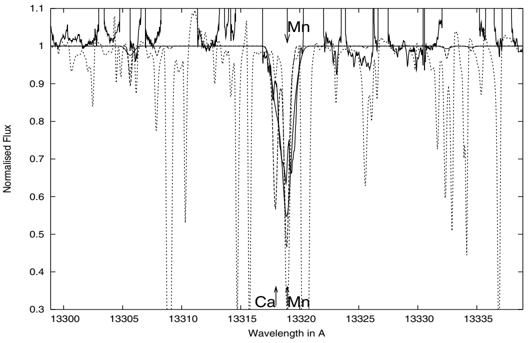
Mn
Ca
Mn
Normalised Flux
1.1
1
0.9
0.8
0.7
0.6
0.5
0.4
0.3
13300
13305
13310
13315
13320
13325
13330
13335
Wavelength in A

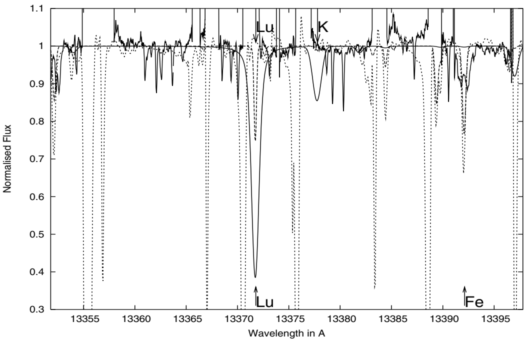
Lu
K
Lu
Fe
Normalised Flux
1.1
1
0.9
0.8
0.7
0.6
0.5
0.4
0.3
13355
13360
13365
13370
13375
13380
13385
13390
13395
Wavelength in A

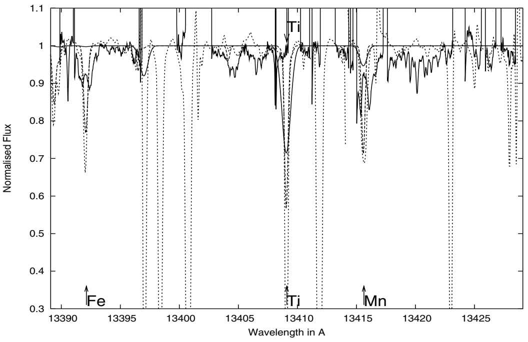
Ti
Fe
Ti
Mn
Normalised Flux
1.1
1
0.9
0.8
0.7
0.6
0.5
0.4
0.3
13390
13395
13400
13405
13410
13415
13420
13425
Wavelength in A

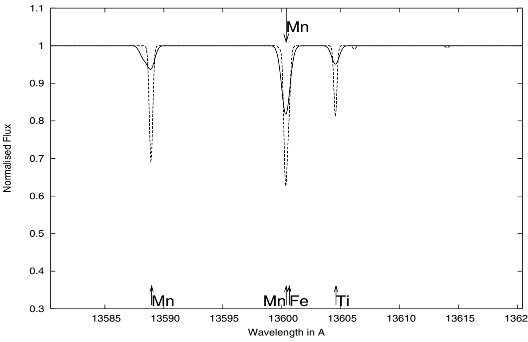
Mn
Mn
Mn
Fe
Ti
Normalised Flux
1.1
1
0.9
0.8
0.7
0.6
0.5
0.4
0.3
13585
13590
13595
13600
13605
13610
13615
13620
Wavelength in A

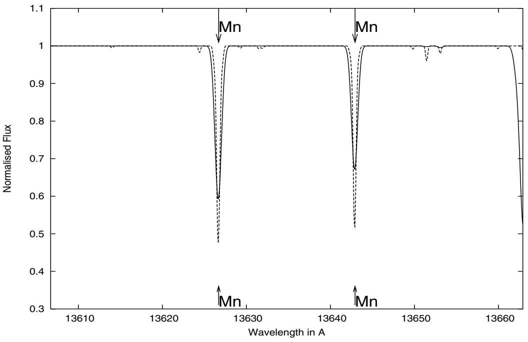
Mn
Mn
Mn
Mn
Normalised Flux
1.1
1
0.9
0.8
0.7
0.6
0.5
0.4
0.3
13610
13620
13630
13640
13650
13660
Wavelength in A

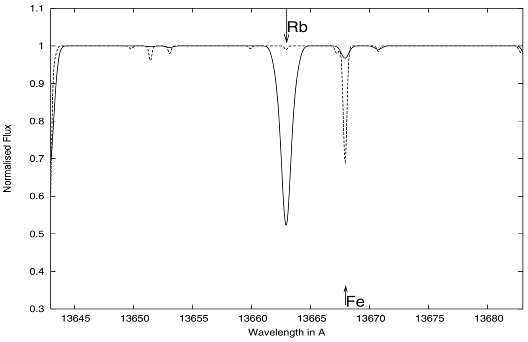
Rb
Fe
Normalised Flux
1.1
1
0.9
0.8
0.7
0.6
0.5
0.4
0.3
13645
13650
13655
13660
13665
13670
13675
13680
Wavelength in A

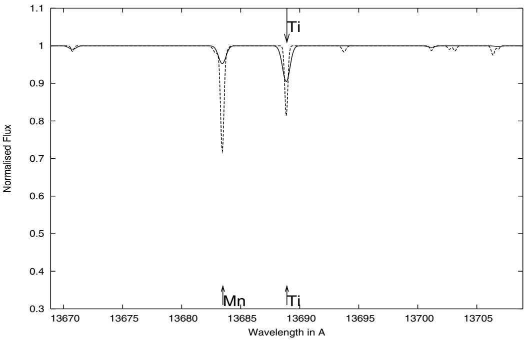
Ti
Mn
Ti
Normalised Flux
1.1
1
0.9
0.8
0.7
0.6
0.5
0.4
0.3
13670
13675
13680
13685
13690
13695
13700
13705
Wavelength in A

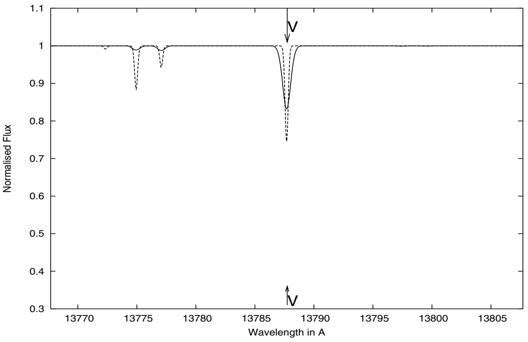
V
V
Normalised Flux
1.1
1
0.9
0.8
0.7
0.6
0.5
0.4
0.3
13770
13775
13780
13785
13790
13795
13800
13805
Wavelength in A

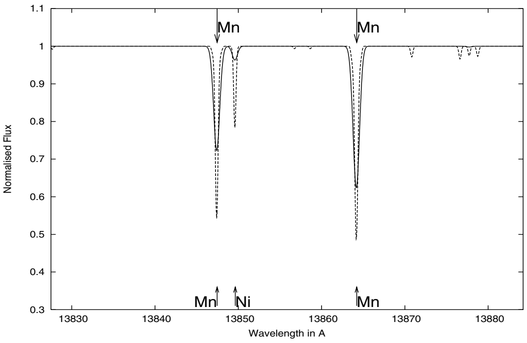
Mn
Mn
Mn
Ni
Mn
Normalised Flux
Wavelength in A
1.1
1
0.9
0.8
0.7
0.6
0.5
0.4
0.3
13830
13840
13850
13860
13870
13880

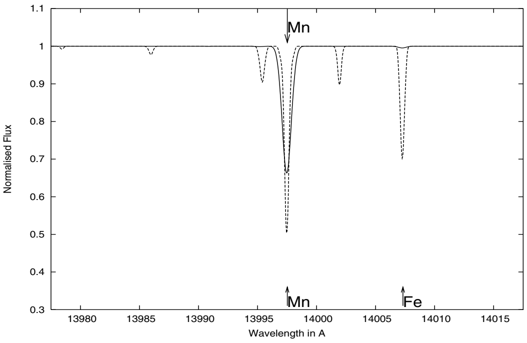
Mn
Mn
Fe
Normalised Flux
Wavelength in A
1.1
1
0.9
0.8
0.7
0.6
0.5
0.4
0.3
13980
13985
13990
13995
14000
14005
14010
14015

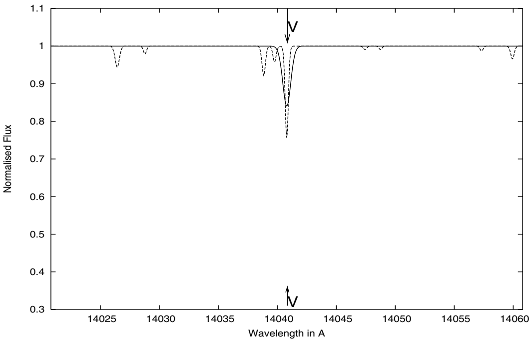
V
V
Normalised Flux
Wavelength in A
1.1
1
0.9
0.8
0.7
0.6
0.5
0.4
0.3
14025
14030
14035
14040
14045
14050
14055
14060

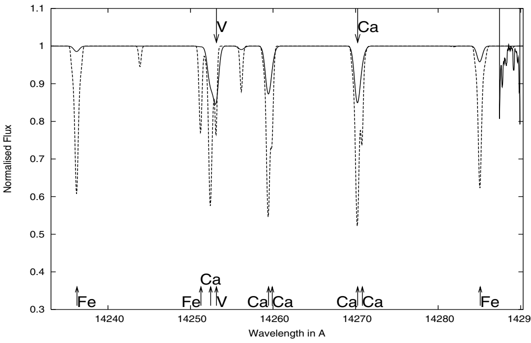
V
Ca
Fe
Fe
Ca
V
Ca
Ca
Ca
Ca
Fe
Normalised Flux
Wavelength in A
1.1
1
0.9
0.8
0.7
0.6
0.5
0.4
0.3
14240
14250
14260
14270
14280
14290

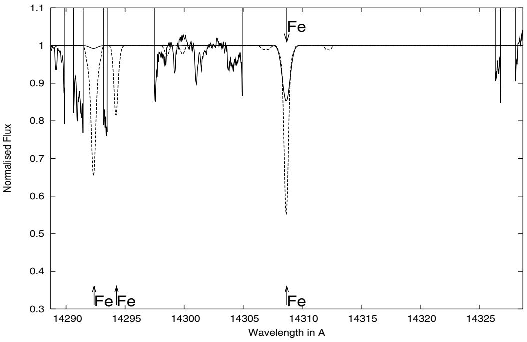
Fe
Fe
Fe
Fe
Normalised Flux
Wavelength in A
1.1
1
0.9
0.8
0.7
0.6
0.5
0.4
0.3
14290
14295
14300
14305
14310
14315
14320
14325

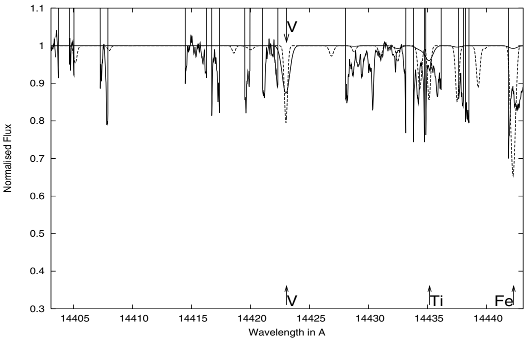
V
V
Ti
Fe
Normalised Flux
Wavelength in A
1.1
1
0.9
0.8
0.7
0.6
0.5
0.4
0.3
14405
14410
14415
14420
14425
14430
14435
14440

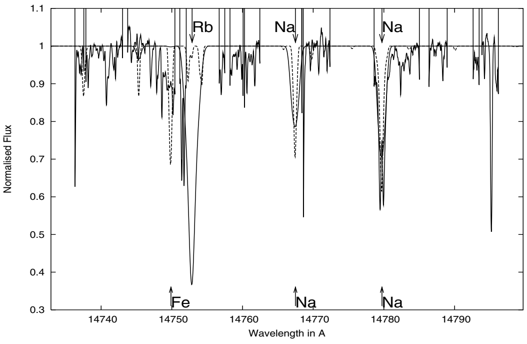
Rb
Na
Na
Fe
Na
Na
Normalised Flux
Wavelength in A
1.1
1
0.9
0.8
0.7
0.6
0.5
0.4
0.3
14740
14750
14760
14770
14780
14790

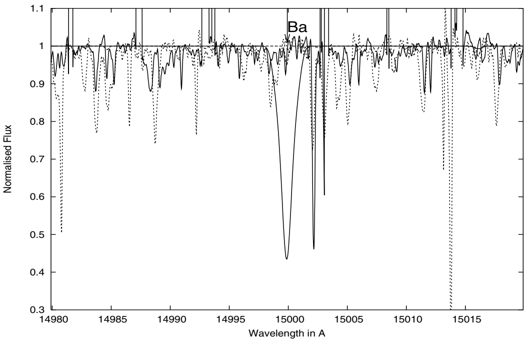
Ba
Normalised Flux
Wavelength in A
1.1
1
0.9
0.8
0.7
0.6
0.5
0.4
0.3
14980
14985
14990
14995
15000
15005
15010
15015

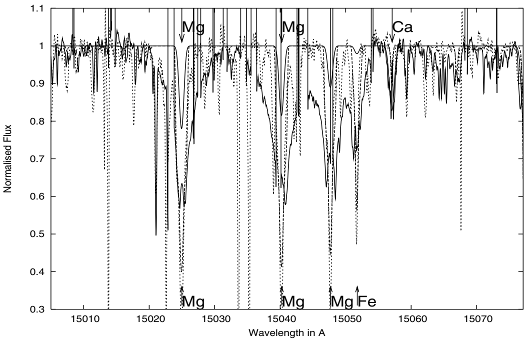
Mg
Mg
Ca
Mg
Mg
Mg
Fe
Normalised Flux
Wavelength in A
1.1
1
0.9
0.8
0.7
0.6
0.5
0.4
0.3
15010
15020
15030
15040
15050
15060
15070

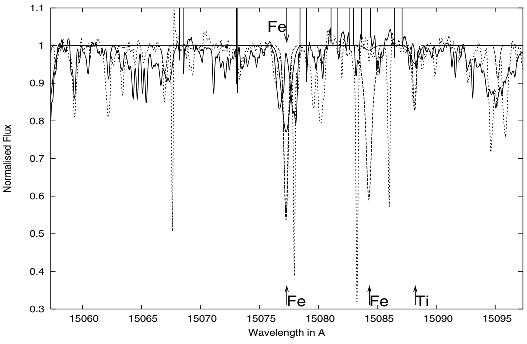
Fe
Fe
Fe
Ti
Normalised Flux
Wavelength in A
1.1
1
0.9
0.8
0.7
0.6
0.5
0.4
0.3
15060
15065
15070
15075
15080
15085
15090
15095

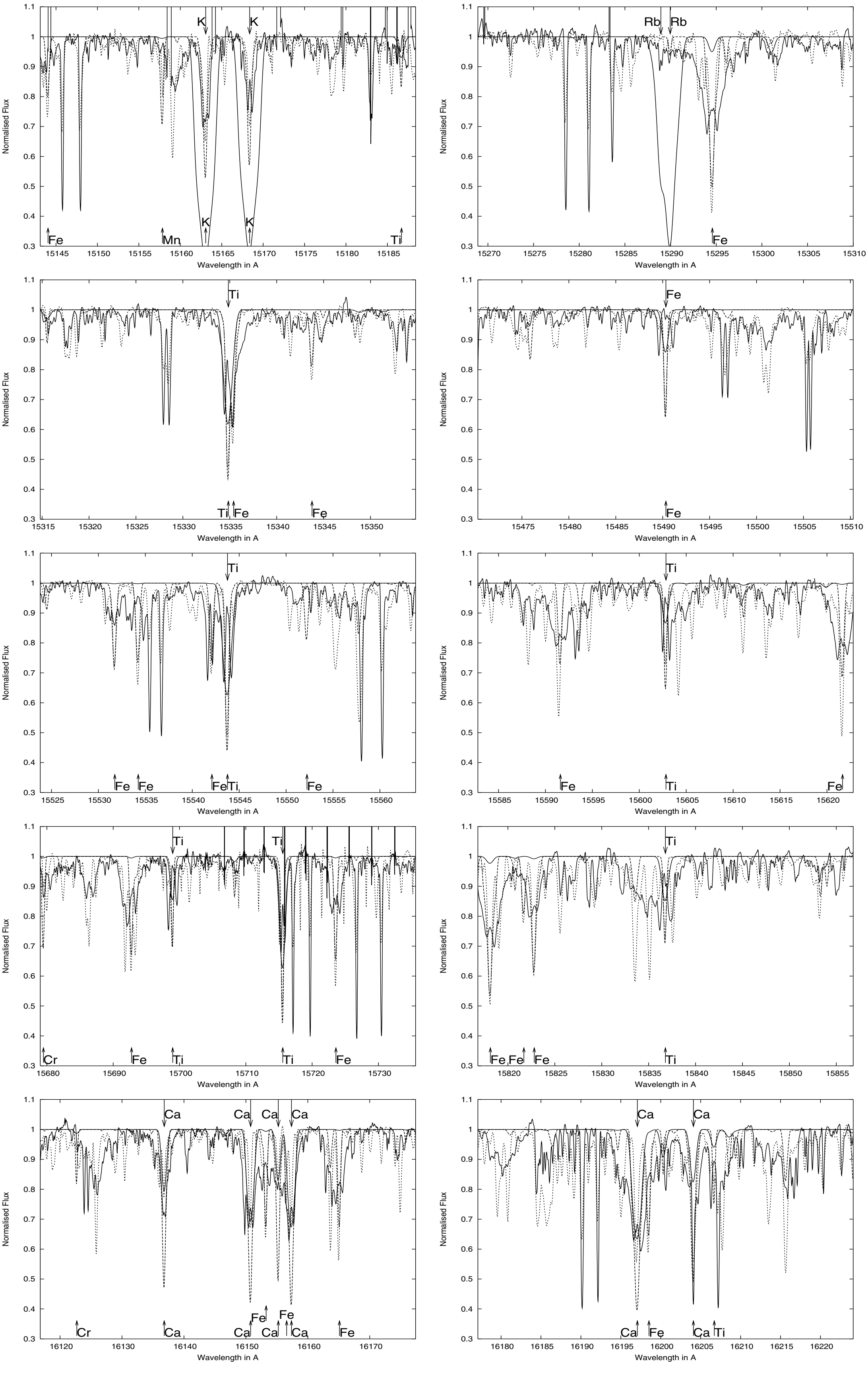
Normalised Flux
Wavelength in A
K
K
Fe
Mn
K
K
Ti
Rb
Rb
Fe
Ti
Ti
Fe
Fe
Fe
Fe
Ti
Fe
Fe
Fe
Ti
Fe
Ti
Fe
Ti
Fe
Ti
Ti
Ti
Cr
Fe
Ti
Ti
Fe
Ti
Fe
Fe
Fe
Ti
Ca
Ca
Ca
Ca
Cr
Ca
Ca
Fe
Ca
Fe
Ca
Fe
Ca
Ca
Ca
Fe
Ca
Ti

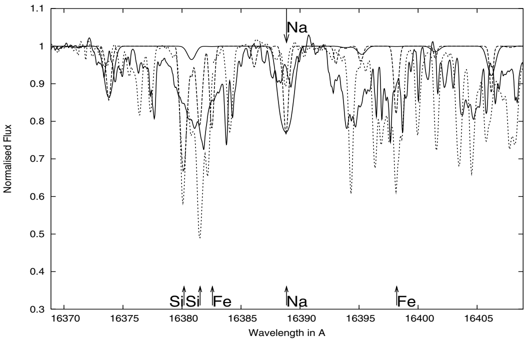
Na
Si Si Fe Na Fe
1.1
1
0.9
0.8
0.7
0.6
0.5
0.4
0.3
Normalised Flux
16370 16375 16380 16385 16390 16395 16400 16405
Wavelength in A

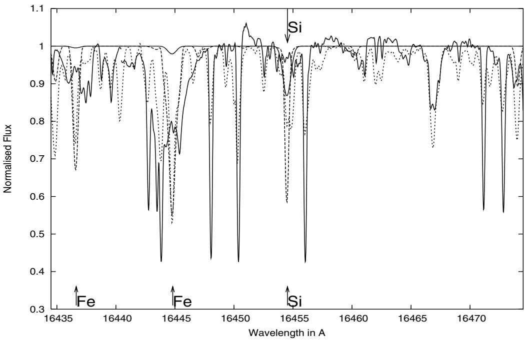
Si
Fe Fe Si
1.1
1
0.9
0.8
0.7
0.6
0.5
0.4
0.3
Normalised Flux
16435 16440 16445 16450 16455 16460 16465 16470
Wavelength in A

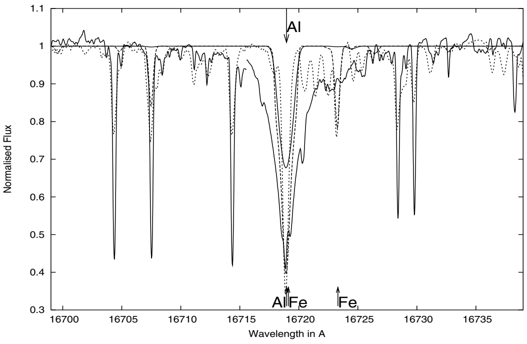
Al
Al Fe Fe
1.1
1
0.9
0.8
0.7
0.6
0.5
0.4
0.3
Normalised Flux
16700 16705 16710 16715 16720 16725 16730 16735
Wavelength in A

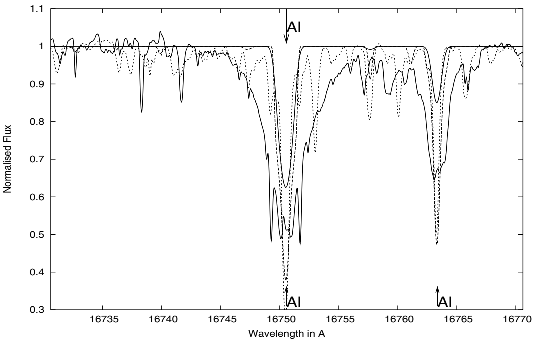
Al
Al Al
1.1
1
0.9
0.8
0.7
0.6
0.5
0.4
0.3
Normalised Flux
16735 16740 16745 16750 16755 16760 16765 16770
Wavelength in A

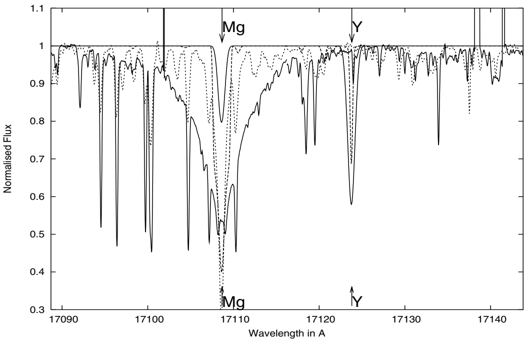
Mg Y
Mg Y
1.1
1
0.9
0.8
0.7
0.6
0.5
0.4
0.3
Normalised Flux
17090 17100 17110 17120 17130 17140
Wavelength in A

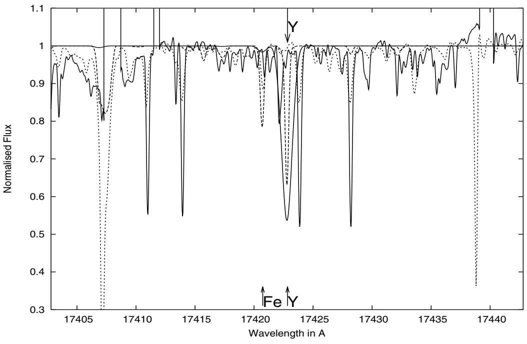
Y
Fe Y
1.1
1
0.9
0.8
0.7
0.6
0.5
0.4
0.3
Normalised Flux
17405 17410 17415 17420 17425 17430 17435 17440
Wavelength in A

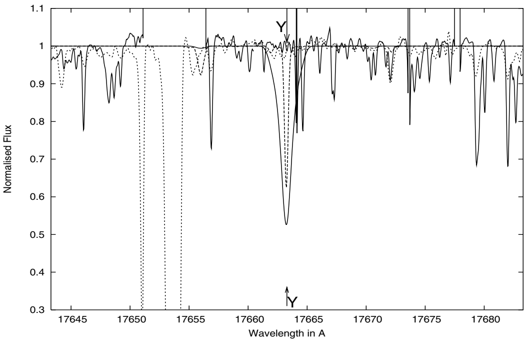
Y
Y
1.1
1
0.9
0.8
0.7
0.6
0.5
0.4
0.3
Normalised Flux
17645 17650 17655 17660 17665 17670 17675 17680
Wavelength in A

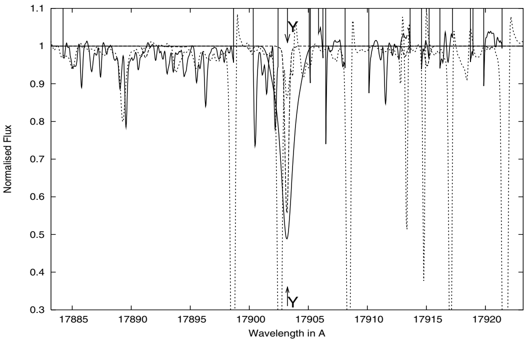
Y
Y
1.1
1
0.9
0.8
0.7
0.6
0.5
0.4
0.3
Normalised Flux
17885 17890 17895 17900 17905 17910 17915 17920
Wavelength in A

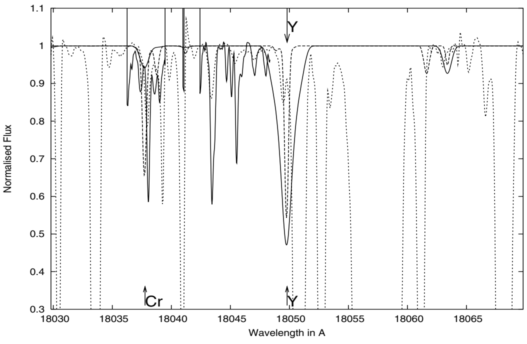
Y
Cr Y
1.1
1
0.9
0.8
0.7
0.6
0.5
0.4
0.3
Normalised Flux
18030 18035 18040 18045 18050 18055 18060 18065
Wavelength in A

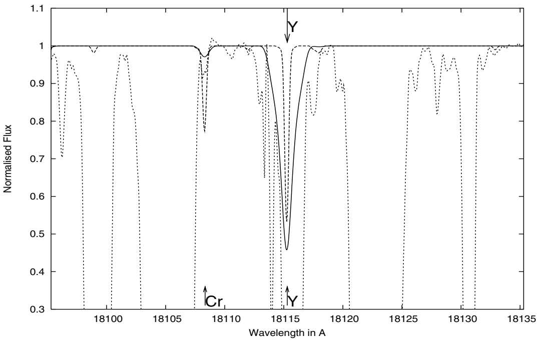
Y
Cr Y
1.1
1
0.9
0.8
0.7
0.6
0.5
0.4
0.3
Normalised Flux
18100 18105 18110 18115 18120 18125 18130 18135
Wavelength in A

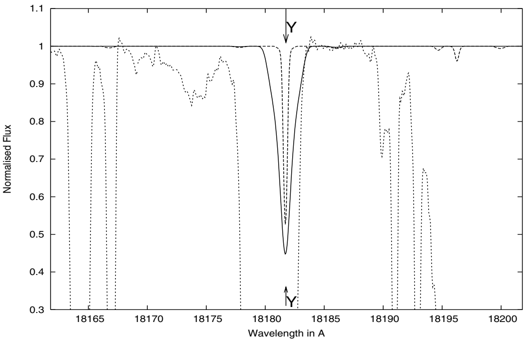
Y
Y
Normalised Flux
1.1
1
0.9
0.8
0.7
0.6
0.5
0.4
0.3
18165
18170
18175
18180
18185
18190
18195
18200
Wavelength in A

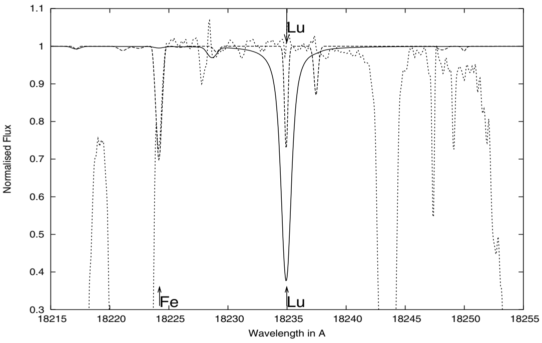
Lu
Fe
Lu
Normalised Flux
1.1
1
0.9
0.8
0.7
0.6
0.5
0.4
0.3
18215
18220
18225
18230
18235
18240
18245
18250
18255
Wavelength in A

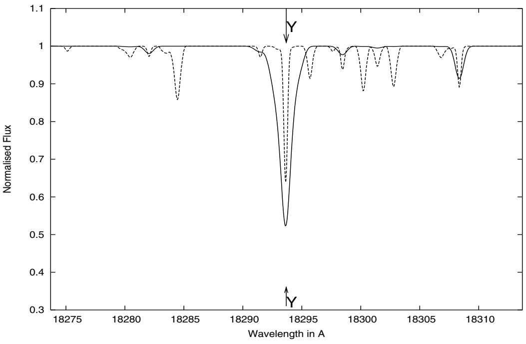
Y
Y
Normalised Flux
1.1
1
0.9
0.8
0.7
0.6
0.5
0.4
0.3
18275
18280
18285
18290
18295
18300
18305
18310
Wavelength in A

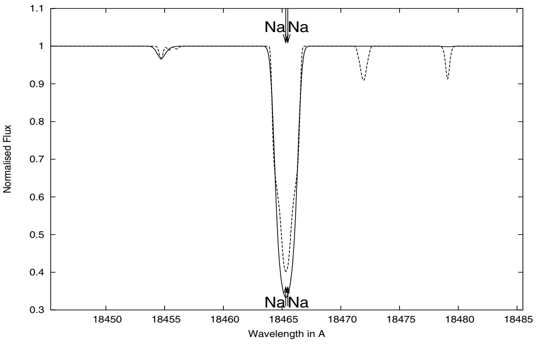
Na Na
Na Na
Normalised Flux
1.1
1
0.9
0.8
0.7
0.6
0.5
0.4
0.3
18450
18455
18460
18465
18470
18475
18480
18485
Wavelength in A

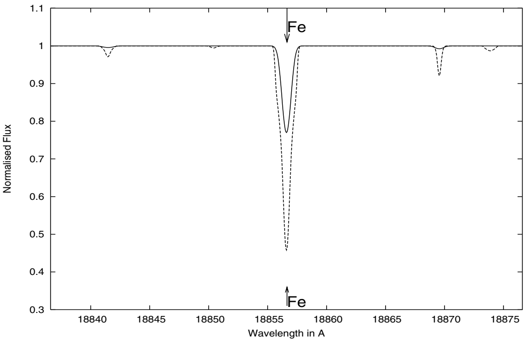
Fe
Fe
Normalised Flux
1.1
1
0.9
0.8
0.7
0.6
0.5
0.4
0.3
18840
18845
18850
18855
18860
18865
18870
18875
Wavelength in A

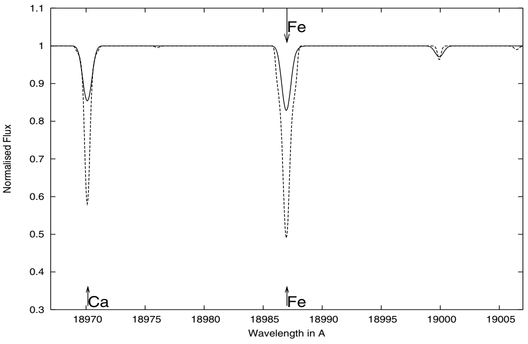
Fe
Ca
Fe
Normalised Flux
1.1
1
0.9
0.8
0.7
0.6
0.5
0.4
0.3
18970
18975
18980
18985
18990
18995
19000
19005
Wavelength in A

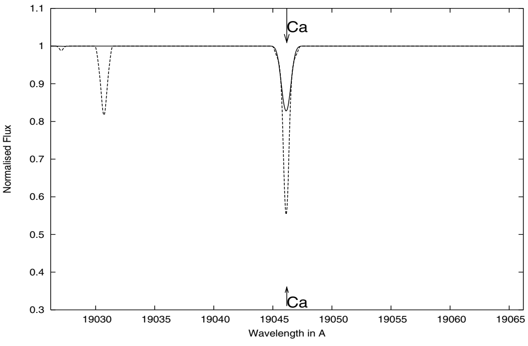
Ca
Ca
Normalised Flux
1.1
1
0.9
0.8
0.7
0.6
0.5
0.4
0.3
19030
19035
19040
19045
19050
19055
19060
19065
Wavelength in A

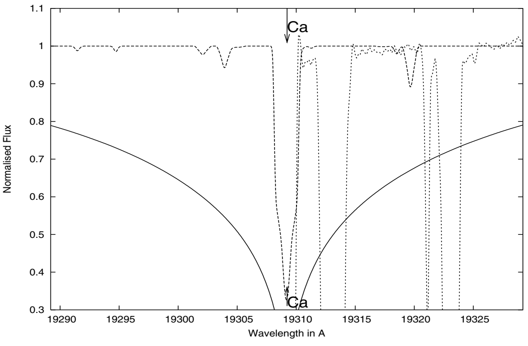
Ca
Ca
Normalised Flux
1.1
1
0.9
0.8
0.7
0.6
0.5
0.4
0.3
19290
19295
19300
19305
19310
19315
19320
19325
Wavelength in A

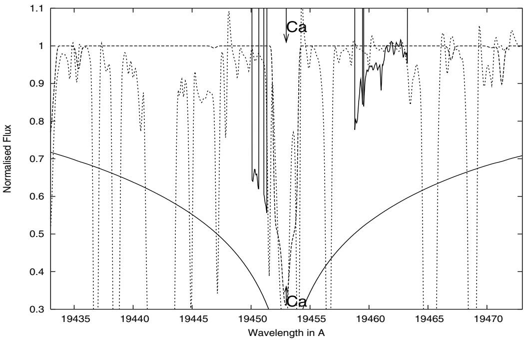
Ca
Ca
Normalised Flux
1.1
1
0.9
0.8
0.7
0.6
0.5
0.4
0.3
19435
19440
19445
19450
19455
19460
19465
19470
Wavelength in A

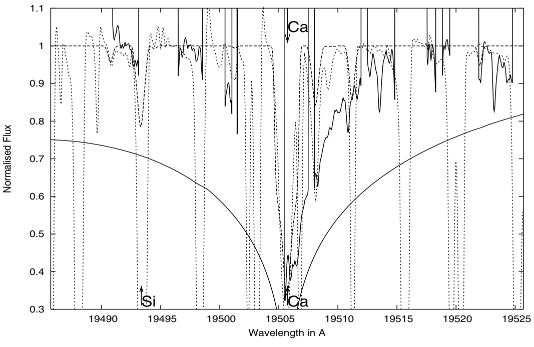
Ca
Si
Ca
Normalised Flux
1.1
1
0.9
0.8
0.7
0.6
0.5
0.4
0.3
19490
19495
19500
19505
19510
19515
19520
19525
Wavelength in A

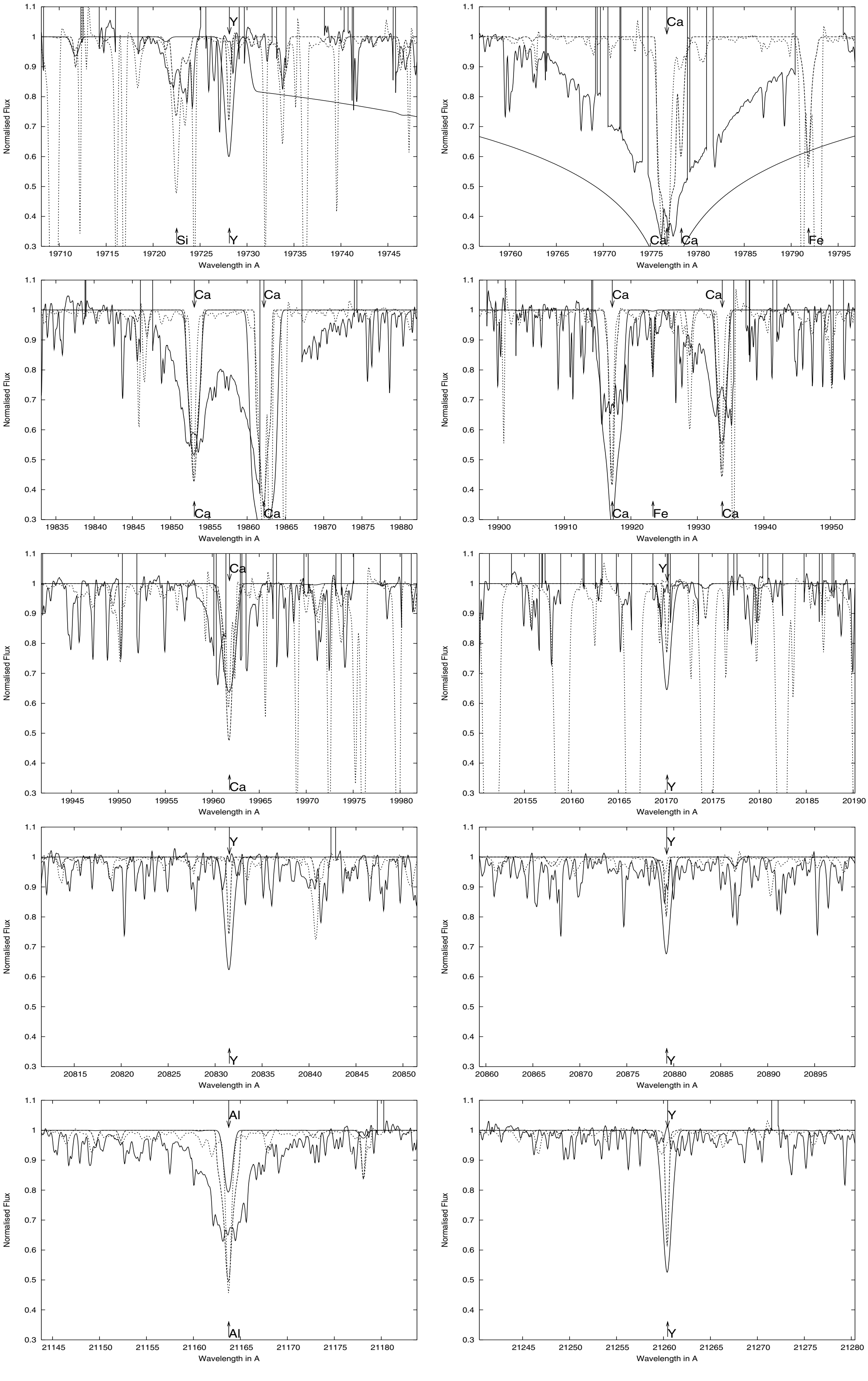
Normalised Flux
Wavelength in A
Si
Y
19710 19715 19720 19725 19730 19735 19740 19745
Ca
Fe
19760 19765 19770 19775 19780 19785 19790 19795
19835 19840 19845 19850 19855 19860 19865 19870 19875 19880
19900 19910 19920 19930 19940 19950
19945 19950 19955 19960 19965 19970 19975 19980
20155 20160 20165 20170 20175 20180 20185 20190
20815 20820 20825 20830 20835 20840 20845 20850
20860 20865 20870 20875 20880 20885 20890 20895
Al
21145 21150 21155 21160 21165 21170 21175 21180
21245 21250 21255 21260 21265 21270 21275 21280
0.3 0.4 0.5 0.6 0.7 0.8 0.9 1 1.1

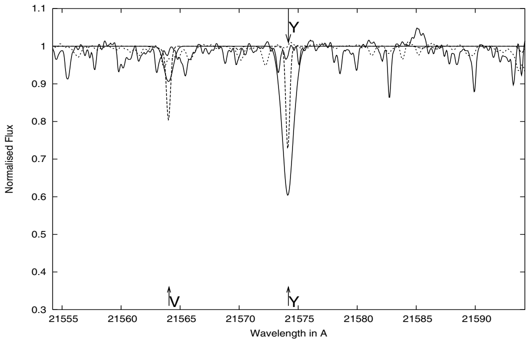
Y
V
Y
1.1
1
0.9
0.8
0.7
0.6
0.5
0.4
0.3
Normalised Flux
21555
21560
21565
21570
21575
21580
21585
21590
Wavelength in A

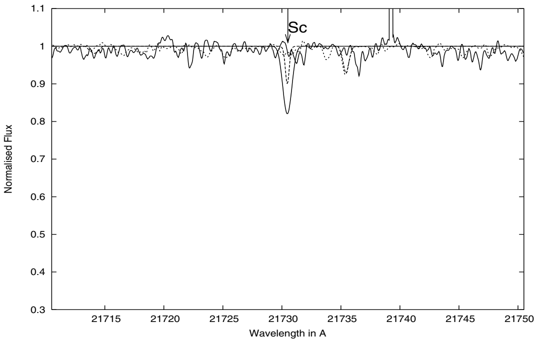
Sc
1.1
1
0.9
0.8
0.7
0.6
0.5
0.4
0.3
Normalised Flux
21715
21720
21725
21730
21735
21740
21745
21750
Wavelength in A

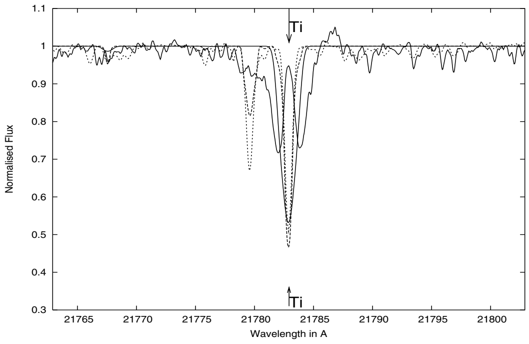
Ti
Ti
1.1
1
0.9
0.8
0.7
0.6
0.5
0.4
0.3
Normalised Flux
21765
21770
21775
21780
21785
21790
21795
21800
Wavelength in A

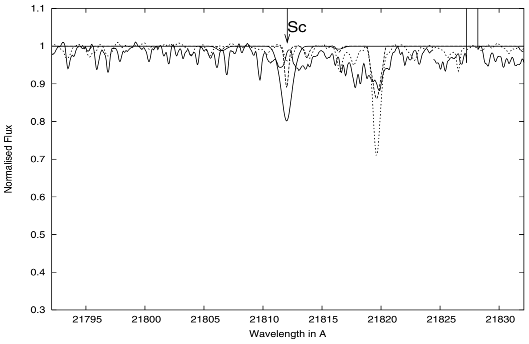
Sc
1.1
1
0.9
0.8
0.7
0.6
0.5
0.4
0.3
Normalised Flux
21795
21800
21805
21810
21815
21820
21825
21830
Wavelength in A

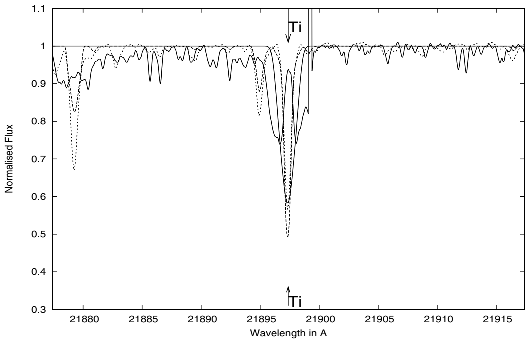
Ti
Ti
1.1
1
0.9
0.8
0.7
0.6
0.5
0.4
0.3
Normalised Flux
21880
21885
21890
21895
21900
21905
21910
21915
Wavelength in A

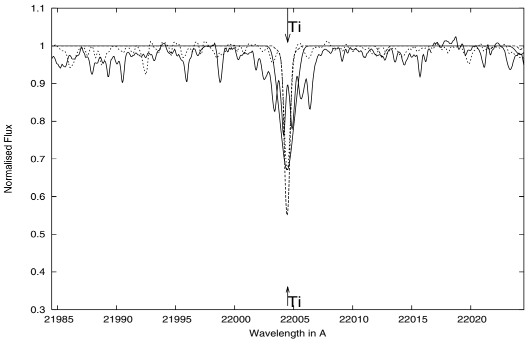
Ti
Ti
1.1
1
0.9
0.8
0.7
0.6
0.5
0.4
0.3
Normalised Flux
21985
21990
21995
22000
22005
22010
22015
22020
Wavelength in A

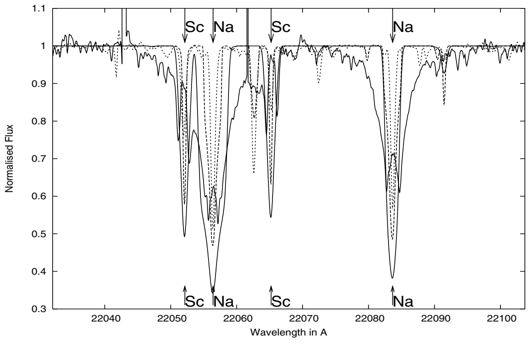
Sc
Na
Sc
Na
Sc
Na
Sc
Na
1.1
1
0.9
0.8
0.7
0.6
0.5
0.4
0.3
Normalised Flux
22040
22050
22060
22070
22080
22090
22100
Wavelength in A

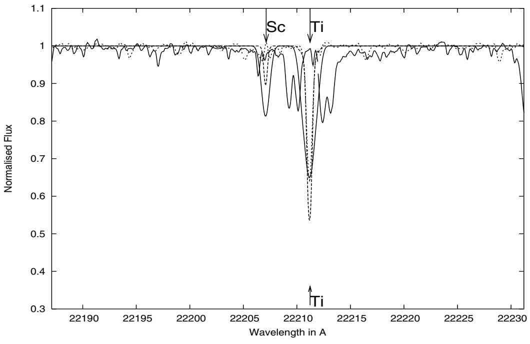
Sc
Ti
Ti
1.1
1
0.9
0.8
0.7
0.6
0.5
0.4
0.3
Normalised Flux
22190
22195
22200
22205
22210
22215
22220
22225
22230
Wavelength in A

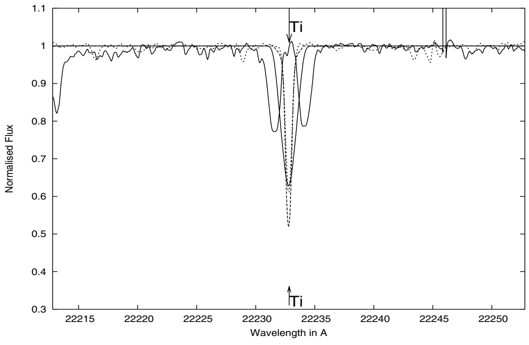
Ti
Ti
1.1
1
0.9
0.8
0.7
0.6
0.5
0.4
0.3
Normalised Flux
22215
22220
22225
22230
22235
22240
22245
22250
Wavelength in A

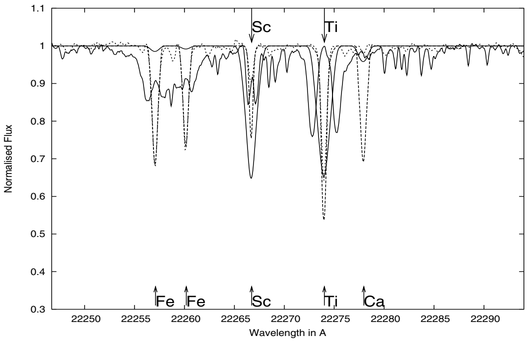
Sc
Ti
Fe
Fe
Sc
Ti
Ca
1.1
1
0.9
0.8
0.7
0.6
0.5
0.4
0.3
Normalised Flux
22250
22255
22260
22265
22270
22275
22280
22285
22290
Wavelength in A

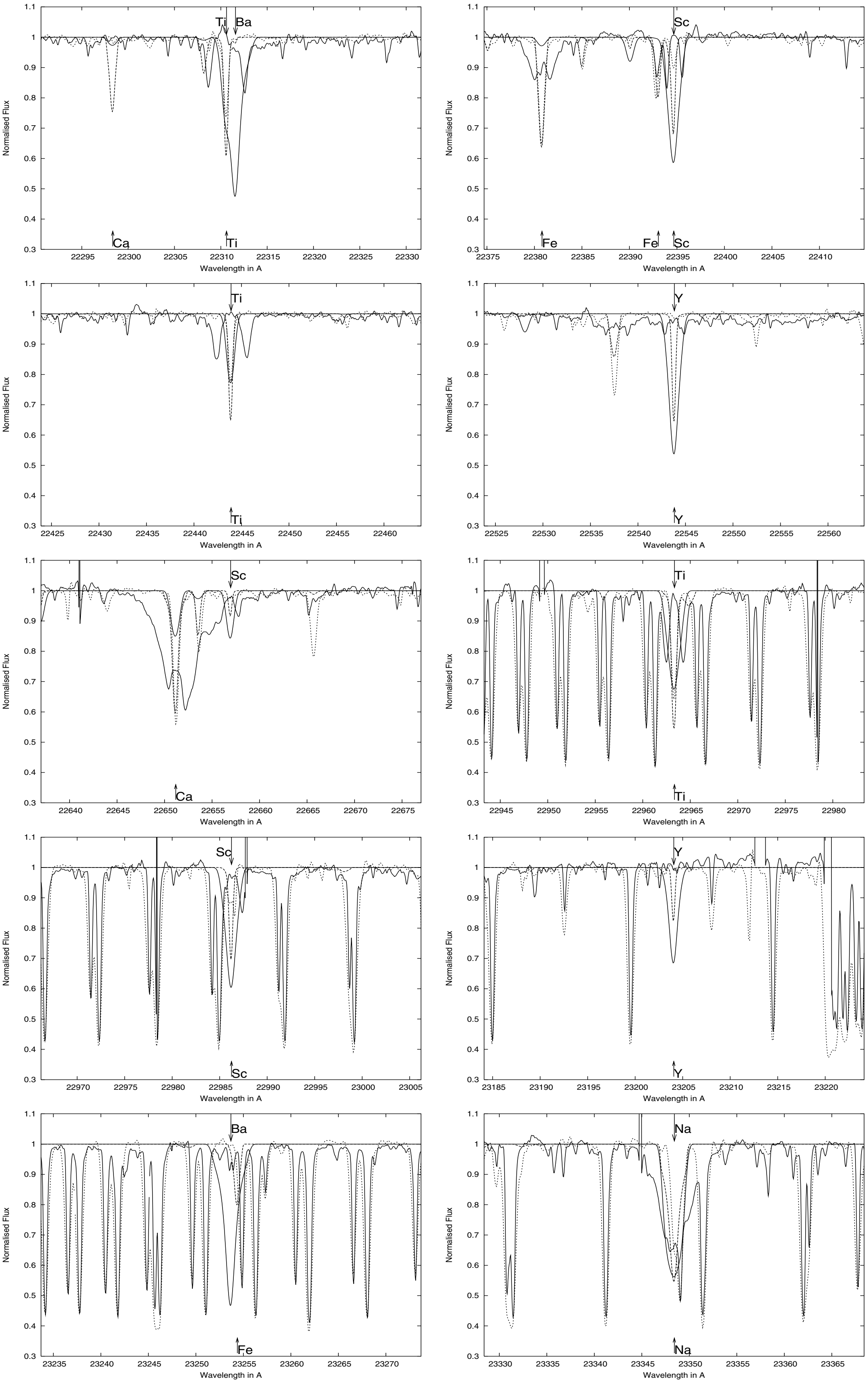
Normalised Flux
Wavelength in A
0.3
0.4
0.5
0.6
0.7
0.8
0.9
1
1.1
Ti
Ba
Ca
Ti
22295
22300
22305
22310
22315
22320
22325
22330
Sc
Fe
Fe
Sc
22375
22380
22385
22390
22395
22400
22405
22410
Ti
Ti
22425
22430
22435
22440
22445
22450
22455
22460
Y
Y
22525
22530
22535
22540
22545
22550
22555
22560
Sc
Ca
22640
22645
22650
22655
22660
22665
22670
22675
Ti
Ti
22945
22950
22955
22960
22965
22970
22975
22980
Sc
Sc
22970
22975
22980
22985
22990
22995
23000
23005
Y
Y
23185
23190
23195
23200
23205
23210
23215
23220
Ba
Fe
23235
23240
23245
23250
23255
23260
23265
23270
Na
Na
23330
23335
23340
23345
23350
23355
23360
23365

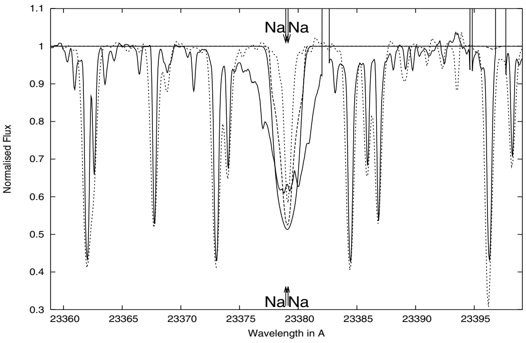
Na Na
Na Na
Normalised Flux
1.1
1
0.9
0.8
0.7
0.6
0.5
0.4
0.3
23360
23365
23370
23375
23380
23385
23390
23395
Wavelength in A

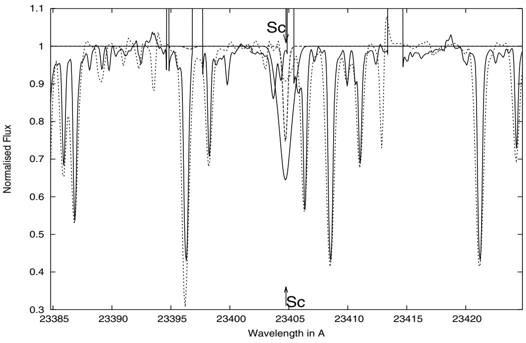
Sc
Sc
Normalised Flux
1.1
1
0.9
0.8
0.7
0.6
0.5
0.4
0.3
23385
23390
23395
23400
23405
23410
23415
23420
Wavelength in A

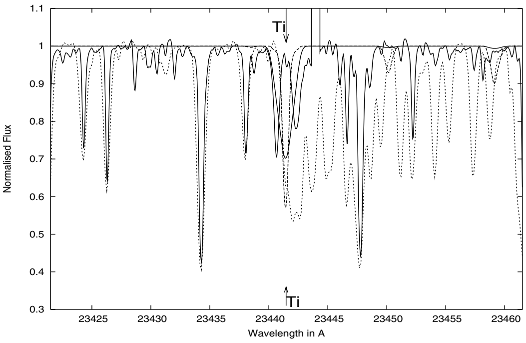
Ti
Ti
Normalised Flux
1.1
1
0.9
0.8
0.7
0.6
0.5
0.4
0.3
23425
23430
23435
23440
23445
23450
23455
23460
Wavelength in A

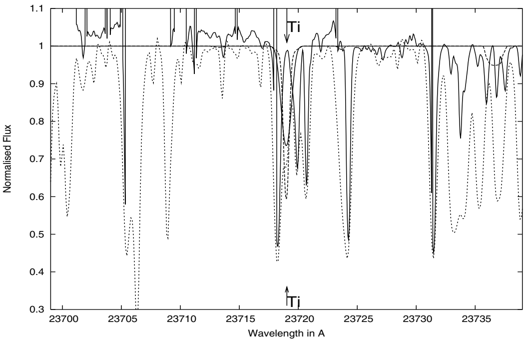
Ti
Ti
Normalised Flux
1.1
1
0.9
0.8
0.7
0.6
0.5
0.4
0.3
23700
23705
23710
23715
23720
23725
23730
23735
Wavelength in A

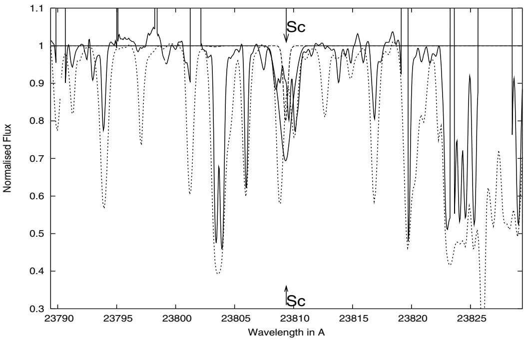
Sc
Sc
Normalised Flux
1.1
1
0.9
0.8
0.7
0.6
0.5
0.4
0.3
23790
23795
23800
23805
23810
23815
23820
23825
Wavelength in A

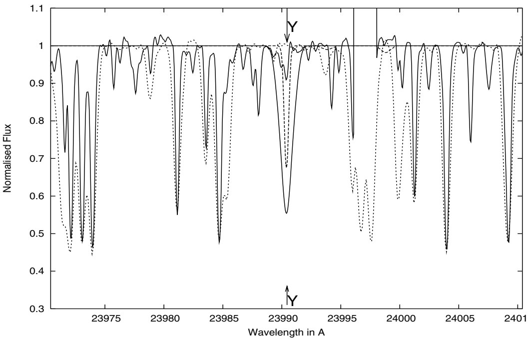
Y
Y
Normalised Flux
1.1
1
0.9
0.8
0.7
0.6
0.5
0.4
0.3
23975
23980
23985
23990
23995
24000
24005
24010
Wavelength in A

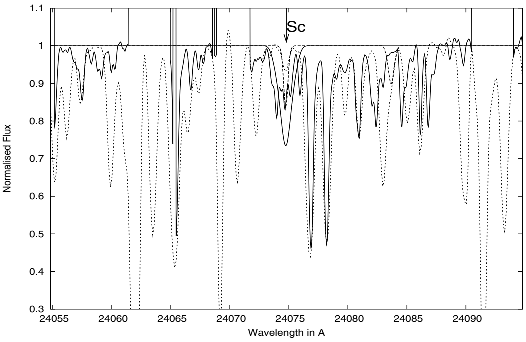
Sc
Normalised Flux
1.1
1
0.9
0.8
0.7
0.6
0.5
0.4
0.3
24055
24060
24065
24070
24075
24080
24085
24090
Wavelength in A

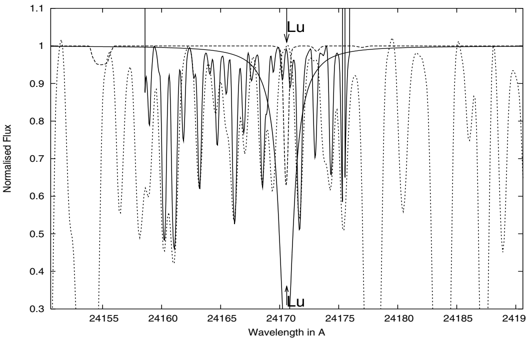
Lu
Lu
Normalised Flux
1.1
1
0.9
0.8
0.7
0.6
0.5
0.4
0.3
24155
24160
24165
24170
24175
24180
24185
24190
Wavelength in A

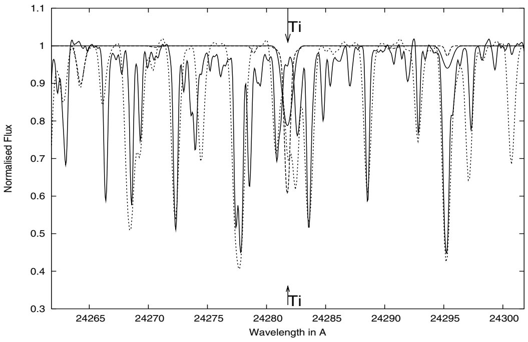
Ti
Ti
Normalised Flux
1.1
1
0.9
0.8
0.7
0.6
0.5
0.4
0.3
24265
24270
24275
24280
24285
24290
24295
24300
Wavelength in A